INVESTIGATING DAMAGE IN REINFORCED CONCRETE MEMBERS USING A VIBRATING WIRE STRAIN GAUGE

Final Year Project UG 2018

By

Hussain Ahmad Sheikh (GL)	00000259631
Sadam Hussain	00000242232
Asad Nadeem	00000268566
Muhammad Usman	00000265896

Supervisor

Dr. Muhammad Usman Hanif

NUST Institute of Civil Engineering (NICE)

SCHOOL OF CIVIL AND ENVIRONMENTAL ENGINEERING (SCEE)

NATIONAL UNIVERSITY OF SCIENCES AND TECHNOLOGY (NUST)

ISLAMABAD

JUNE 2022

This is to clarify that the

FINAL YEAR PROJECT TITLED

INVESTIGATING DAMAGE IN REINFORCED CONCRETE MEMBERS USING A VIBRATING WIRE STRAIN GAUGE

Submitted By

Hussain Ahmad Sheikh (GL)	00000259631
Sadam Hussain	00000242232
Asad Nadeem	00000268566
Muhammad Usman	00000265896

Has been accepted towards the requirements for the undergraduate degree in

Civil Engineering

_____

Thesis Supervisor:

Dr Muhammad Usman Hanif

Thesis Supervisor's Signature:_____

NUST Institute of Civil Engineering (NICE)

SCHOOL OF CIVIL AND ENVIRONMENTAL ENGINEERING (SCEE)

NATIONAL UNIVERSITY OF SCIENCES AND TECHNOLOGY (NUST)

ISLAMABAD

JUNE 2022

Declaration

I certify that this Final Year Project titled “Investigating Damage in Reinforced Concrete Members Using a Vibrating Wire Strain Gauge*”* is my own work. The work is unique and has never been evaluated before. The material that has been used from other sources has been properly acknowledged/referred

Signature of Student: _____

Hussain Ahmad Sheikh

(Group Leader)

Acknowledgements

In the name of Allah, the most beneficent the most merciful. All praise is to Allah due to whom the completion of our project was possible.

We are greatly gratified by the guidance provided to us by our respectable advisor, **Dr Muhammad Usman Hanif**. He dedicated his time and energy towards us so that we were always free of doubts. It was due to his encouragement that we remained motivated till the end.

Moreover, we are thankful towards are co-advisor, **Dr Usman Hassan**, who provided us with his valuable suggestions. We would also like to mention our families and seniors whose constant prayers and well wishes were alongside us from the very first day.

We extend our profound gratitude towards the teaching faculty of Structural Engineering at NUST Institute of Civil Engineering (NICE) who were always ready to provide us with their positive feedback.

Dedicated To

Our Supervisor Dr Muhammad Usman Hanif

&

Our families

Abstract

Recently the use of vibrating wire strain gauges has increased to find out the damage in a reinforced concrete structure. The assembly and functioning of this acoustic strain gauge are presented. This gauge provides numerous benefits including its sensitivity to measure strain (up to 1micron) and its property of being easily attached on any concrete surface. The gauge apparatus can be made in a lab due to its low cost which gives it an edge over the conventional systems. The gauge was calibrated after considering the variations in temperature.

The purpose of the experimentation was to record the changes in nonlinear vibrations with respect to the damage caused in the reinforced concrete member. These changes were later studied using the vibration tests on the reinforced concrete beam. Non-linearities were observed by the changes in the fundamental frequency. Discrete Fourier transforms moving window was utilized to analyze the vibration signals specifically the change in frequency with respect to time. The results are presented and reviewed.

Keywords:

- Strain Gauge
- Reinforced Concrete Structures
- Non-linear Vibrations
- Natural Frequency
- Fundamental Frequency
- Fourier Transformation
- Vibration Signals
- Temperature Variations

Table of Contents

List of Figures

CHAPTER 1

INTRODUCTION

1.1 Background

Recently there has been a great development in the field of damage assessment at the early stages of a reinforced structure. Traditional methods revolve either around detecting cracks visually or using localized experimental methods such as ultrasonic and acoustic techniques. The requirement of these methods is that the precise location of the cracks is recognized and approachable. Therefore, recent methods primarily focus on the changes that take place in the vibrational properties of the structure itself. However, the existing work that has been done using the vibrational techniques conformed with the assumption that the vibrations are linear. Which meant that the modal properties of the structure did not change with the amplitude of the oscillations.

1.2 Problem Statement

The work discussed here involves the small amplitude behaviour of cracked concrete beams. This involves the need of the measurement of strain in order of tens of $\mu\varepsilon$ to a higher degree of accuracy. The standard electrical resistance gauges are unable to measure at such degrees of accuracy. Moreover, these gauges are not suitable when it comes to attaching them on the concrete surface as they are unable to bridge the cracks. Hence, the vibrating wire strain gauge proves to be a useful alternative. These gauges in comparison to the traditional gauges provide us with strains of accuracy in the order of hundreds of microstrain. Other advantages of the vibrating wire strain gauge include the easiness of attachment and its ability to take measurements with cracks on the specimen.

The vibrating wire strain gauge consists of a pre-tensioned steel wire between two fixed supports attached on the specimen to be assessed. When there is a change in the property of the concrete specimen it brings upon a change in the tension of the wire, resulting in the variation in fundamental frequency. This variation is then to be related to the value of deformation with the help of physical-mathematical models.

One of the limitations of the use of a vibrating wire strain gauge is its sensitivity to the variations in temperature. 1˚ change in temperature results in a 20 $\mu\varepsilon$ change in

the strain of the wire. This error is linked with the differences between the thermal expansion coefficients of both the gauge and the concrete specimen.

1.3 Objectives

1. Experimental setup of the gauge
2. Calibration of the gauge
3. Using the gauge for damage assessment

1.4 Thesis Structure

Followed by the introduction, a detailed literature review has been provided in chapter 2 which discusses the linear and non-linear responses of vibrations. Chapter 3 explains time-frequency analysis which includes the Nyquist theorem, Leakage and Fourier transformations. In chapter 5 theory of vibrating wire strain gauge, frequency strain relationship and effect of temperature on frequency of wire are explained in detail. Chapter 5 explains the methodology of our research which discusses in detail the process of how temperature correction was achieved, and the signal processing techniques involved. Further, the method of gauge calibration and the use of the gauge itself is presented. Later, in chapter 6 results and conclusions are discussed.

CHAPTER 2

Literature Review

The testing techniques based on vibrations can be divided into two parts: those who consider vibration as

1. Linear response
2. Non-linear response

Firstly, we will discuss linear vibration response and then nonlinear methods will be explained. Then we will discuss different possible testing techniques.

2.1 Linear Response Methods

The idea of using vibrations for structural health monitoring was an innovation in damage assessment. This idea is worked on the principle that the damage causes a reduction in stiffness and natural frequency of the civil engineering structures. Most research into using vibration techniques to detect damage looks at modal characteristics and assumes that they are linear, and do not consider the amplitude. The many sorts of indicators can be divided into numerous categories, which are briefly detailed below with some application examples. Some methods are explained below in detail.

2.1.1 Natural Frequencies Method

Variations in natural frequency are a rather insensitive approach to diagnosing the damage, according to the literature.

The researchers named Farrarand Jauregui (Jauregui, 1998) performed a test on a steel plate girder bridge and found that even at significant damage states, there were only minor changes in frequency. The largest change in natural frequency was only 7% at a 96.4% reduction in the stiffness of one of the main girders. There was no discernible variation in frequency at lower damage levels.

Maguire and Severn (Severn, 1987) performed tests on four pre-cast post-tensioned reinforced concrete bridge beams with a span of 27.6 m that were simply supported. When the cover concrete was removed, exposing the pre-stressing tendons, they reported a decrease in frequency. However, the modifications were minor, and their frequency resolution was comparable.

Then Salawu (Salawu, 1997) performed a test on a concrete bridge before the support bearings and after the support bearings were changed and found that the average variation for the first six modes of vibration was just 1.7 percent.

A considerable number of laboratory tests have also been recorded. Eccles et al (B.J. Eccles, 1997). discovered that when concrete beams were damaged by four-point loading, the fundamental frequency decreased by roughly 12 percent at first, however, the change in frequency was only 2.5 percent for additional damage.

The few publications chosen here show that the frequency varies with the severity of the damage and that the frequency reduces as stiffness reduces. But the changes in frequency are minor as compared to oscillations caused by external factors, such as temperature changes. When the atmospheric temperatures were 0°C and 15°C, Abdel Wahab and De Roeck (Roeck, 1997) took two readings of the natural frequency of a prestressed reinforced concrete bridge. The change in natural frequency as a consequence of the temperature rise was roughly 4-5 percent. Roberts (Roberts, 1995) investigated the effects of temperature on the natural frequencies of a reinforced bridge structure for a year and found that temperature was the most significant cause of change in frequency, accounting for 4% of complete change, while a finite element model suggested that damage-related changes could be in the region of 1%. The temperature changes had no substantial effect on mode forms, according to a second important finding.

2.1.2 Method of Damping Ratios

There have been several attempts to use damping ratios as a damage measurement, but they have failed. Although damping ratios were altered by degradation in a steel girder with concrete decking, Salane and Baldwin (Jr., 1990) concluded that they were inadequate indicators since they initially increased and subsequently declined with increasing damage. Farrar and Jauregui (Jauregui, 1998) also discovered that the damping of a steel plate girder bridge did not vary with an increase in the damage consistently.

Salawu and Williams (Williams, 1995) carried out tests on a reinforced concrete bridge before and after structural repairs and determined that the changes in damping for different modes were inconsistent. So, they found that there was no specific relationship between the damage and damping.

2.2 Non-Linear Response Methods

In contrast to a large amount of research that has been done on damage detection through linear methods, little research has been done on time-dependent non-linear vibrational features of civil engineering reinforced concrete structures.

2.2.1 Concrete Beams Non-Linear Testing

There is fever research on the non-linear amplitude-dependent modal characteristics of concrete beams that have been published. Eccles et al (B.J. Eccles, 1997) tested many beams for impact excitation. They demonstrated that when the oscillation amplitude is big, the frequency is initially lower in comparison to when the amplitude is small. When the amplitude is modest, the frequency stabilizes, and no additional amplitude dependency can be noticed. For higher levels of damage, the gradient of increasing frequency with time is larger. However, the fundamental frequency of the beams tested was significantly greater than what is predicted for a bridge, and the excitation of vibration dissipated extremely quickly.

Goldsmith (Goldsmith, 1999) observed that there was a little amplitude dependency while the beam was in undamaged condition, this increased as the beam was damaged up to the point where the rebars started to yield. After rebars yield, the amplitude stopped increasing, and only a decrease in whole frequency was observed. The figure below depicts a frequency vs. time graph for growing damage. The frequency information is determined by the interaction with an impulse detected at time t = 0. The plot with the largest natural frequencies is the undamaged condition, and the average frequency steadily declines as damage rises. The starting decrease in frequency up to roughly 0.025 s is because of the windowing effect inside the adjusted exponential distribution utilized in the data analysis.

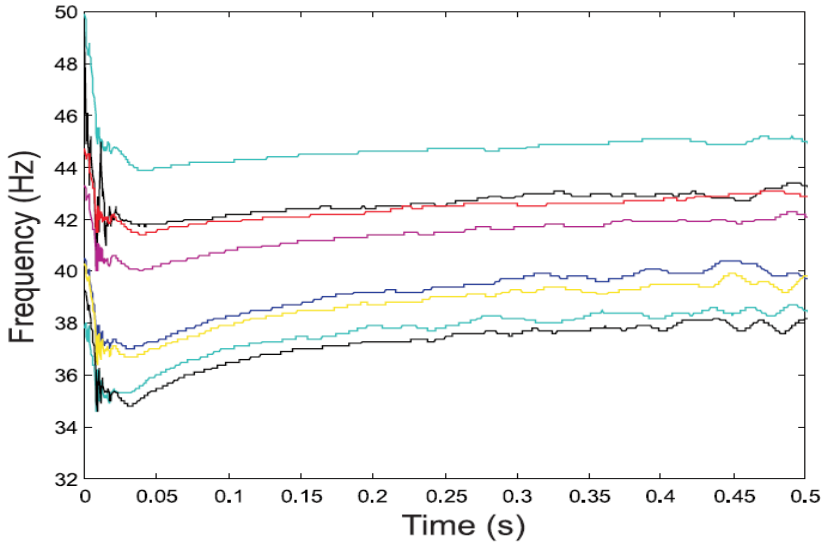

Figure 1: Frequency vs Time

Van Den Abeele and Visscher (Visscher, 2000) carried forced vibration testing. They built a plot of the natural frequencies at various amplitudes of vibration using continuous-wave excitation at varying amplitudes. The testing revealed that while the beams did not act linearly when it was in undamaged condition, the non-linearities became much more significant when the beam was damaged by the application of four-point loading. Owen (Owen, 2001) experimented with this strategy as well. Using time-domain-domain experiments, Van Den Abeele and Visscher found similar patterns. The testing sample was exposed to steady-state excitation near to its natural frequency before the test, and then the excitation was discontinued at the commencement of the test, allowing the natural frequency and decline of the beam to be observed. This test is comparable to the impulsive excitation experiments performed by Eccles et al (B.J. Eccles, 1997). but it has the benefit of activating only one mode at a frequency that is close to an excitation frequency before the start of the test. However, the testing necessitated the use of shaker tools, which increases complexity, especially if it were to be used on a large-scale structure.

Eccles et al (B.J. Eccles J. O., 1999). revealed another potential way of detecting damage. They used a natural frequency to stimulate the beam and observed acceleration for fixed excitation energy. A phase-plane plot could be found by integrating the acceleration data multiple times In the phase plane, the path travelled by a linear system is a circle. The extent to which the computed path deviates from a circle is computed by the system's non-linear response. However,

when displayed in the frequency domain at integral multiples of the excitation frequency, these non-linearities would appear in the signal, which would be easier to comprehend.

2.3 Possible Testing Methods

There has been a lot of research done on the benefits and drawbacks of the three types of tests, including extensive studies by Salawu and Williams (Williams, 1995) and Prakash Rao et al (D.S. Prakash Rao, 1983). There are three primary types of testing methods:

- Forced Vibration
- Impact Excitation
- Ambient Excitation

The bridge is excited over a broad frequency band, at one frequency using a shaker, or a steadily change in frequency in forced vibration tests. The fundamental advantage of vibration tests is that the amplitude can be kept uniform, allowing the periodic response to be averaged over several cycles, resulting in a cleaner response shape. Other benefits of forced vibration tests include knowing the input excitation and being able to regulate the frequency range. A downside is that a big shaker is necessary to excite a bridge at a tolerable amplitude, which raises the expense of the testing. The bridge must also be blocked to prevent vehicle excitement from affecting the tests. Salawu and Williams (Williams, 1995), as well as Kramer et al (Severn, 1987)., conducted forced excitation studies on bridges and found the requirement for using more than one shaker to reduce the influence of vibration due to moving traffic loading.

Raghavendrachar and Aktan (Aktan, 1992), for example, conducted impact excitation tests on a bridge by constructing a hump on the road and driving a truck on it. Although the bridge has to close testing duration as with forced vibration testing, the interruption to traffic is reported to be less because the testing procedure is very efficient in case of impact test, and the bridge can be held open for traffic between tests. The truck movement across the bridge causes a shift in mass distribution, which is a concern with this form of excitation. Humar and Kashif (Kashif, 1993) have done theoretical work to analyze the effect of a truck passing along a bridge. Kramer et al. (C. Kr¨amer, 1999) used a different test method, which involved putting weight

onto the reinforced concrete bridge span. However, this is very complicated than truck excitation and may stop the flow of traffic between testing and measuring the input force is easier. On a small scale, Mazurek and DeWolf (DeWolf, 1990) compared two different methods of impulsive excitation They discovered that the weight of the vehicle affected the natural frequencies by up to 3% and that the shifting distribution of weight modified the damping qualities as the model vehicle traversed the beam. Kramer et al (C. Kr¨amer, 1999). evaluated the three kinds of tests and determined that, despite the lower levels of excitation, drop-weight excitation produced similar modal features as forced excitation testing for the bridge they investigated.

Ambient excitation tests are the simplest and least expensive to conduct, as they rely solely on the flow of traffic or other forms of ambient excitation. There would be no need for costly excitation equipment or traffic disruption, and the bridge vibration could be recorded remotely using permanently placed accelerometers and data-gathering devices. It is, however, the hardest method of stimulation to understand. The mass distribution on the bridge is constantly changing, and the vibration is caused by interaction with the car suspensions. Although Ward has done some effort to tackle this difficulty, the incoming excitation is undefined and must be considered to be white noise. He advised that the vibration response of the road be measured and used to equalize the bridge's reaction. Another issue is whether the ambient stimulation will be large enough to allow measurement of the modal characteristics. Traffic excitation was suitable for measuring the starting 12 modes of a multi-span steel bridge structure, according to Roberts, and sufficient excitation was also adequate to assess the modal characteristics of a short-span concrete bridge, according to Kramer et al.

In field trials, the suitability of different kinds of tests for detecting non-linearities has still not been established.

2.4 Conclusion From Literature Review

A review of the literature reveals that, while some promising work on damage identification in concrete structures using linear approaches has been published, Some significant challenges are still there to overcome, particularly in terms of sensitivity and the impact of external factors. Nonlinear approaches for detecting the dependence of natural frequency on amplitude should be researched further. Eccles et al (B.J. Eccles J. O., 1999). and Goldsmith's (Goldsmith, 1999) work on amplitude-frequency frequency dependence is a suitable beginning place for this research. To imitate drop-

weight experiments on bridges, more impact tests were undertaken on simply supported conditioned beams with less natural frequencies and larger geometry than those employed by Eccles et al (B.J. Eccles J. O., 1999). and Goldsmith (Goldsmith, 1999). This was thought to be superior to forced vibration excitation because it would allow for direct measurement of the beam frequency during the decaying vibration caused by the hit. The work offered here is divided into three sections:

2.4.1 Time-Frequency Distributions

The change in natural frequency of the reinforced beam with time should be evaluated to detect non-linearities in impact loading. The optimal way of analyzing the data was determined after a thorough examination of time-frequency distribution tools.

2.4.2 Modelling

A mathematical non-linear model of a beam capable of evaluating multiple hypothetical crack mechanisms would be important to better understand the explanation for the non-linearity. The types of models have been used to model non-linear cracks in homogeneous materials. Those models, on the other hand, are complicated, relying on fracture mechanics to estimate the distribution of stress in the cracked region, which is further transformed into a spring stiffness. A reinforced concrete beam would be extremely tough to apply this strategy on. As a result, it was considered that a basic vibrating beam model, which allowed for the addition of the moment-rotation connection over a cracked region, would be a helpful addition to the previous study.

2.4.3 Experimental Work

Impact excitation studies were carried out on a reinforced concrete beam having relatively less frequency. The relationship between the frequency of the beam and amplitude of the vibration changed with the increase in damage level, and a method for monitoring the moment-rotation relationship over the fractured region was established. This is expected to be used in conjunction with the model to help researchers better understand the vibration nature of cracked concrete beams.

CHAPTER 3

Time-Frequency Analysis

It is important to be able to compute an estimation of the instant frequency components of the vibration at any moment to find a time-frequency relationship to analyse the non-linear effects of a vibrating beam. Several approaches will be studied in this chapter.

3.1 Nyquist Theorem

The Nyquist theorem is also referred to as the sampling theorem. It is utilized in the digitization of analogue signals. Samples of the analogue waveform are taken consistently to convert the signal from analogue to digital. Sampling rate or frequency is the number of samples taken in a second. The theorem states that a sinusoidal function in time or distance can be redeveloped while preserving the information. This is possible when it is sampled at a frequency equal to or larger than twice per cycle. This is usually the case because of the quantization errors that occur during the sampling process. For example, humans can hear frequencies in the range of 20-20000Hz so that is why the audio signal is sampled at a rate of 40000HZ when music is stored on a CD.

An analogue signal v_a can be recreated from its samples with the help of the equation given by the Nyquist Theorem:

$$v_a(t) = \sum_{k=-\infty}^{\infty} v_a[kT_s] \left[\operatorname{sinc}\left(\frac{t-kT_s}{T_s}\right)\right]$$

3.2 Aliasing:

If the initial samples are not sufficiently closely spaced to represent high-frequency components present in the underlying function, then the DFT values will be corrupted by aliasing. To solve this problem either the sampling rate is increased, or the signal is pre-filtered to reduce the high-frequency spectral content.

3.3 Leakage:

The continuous Fourier transform of a periodic waveform requires the integration to be performed over the interval - infinity to + infinity P or over an integer number of cycles of the waveform. If we attempt to complete the DFT over a non-integer number of cycles of the input signal, then we might expect the transform to be corrupted in some way. To solve the problem of leakage, window functions can be used. This tapers the sample towards zero values at both endpoints eliminating discontinuity with a hypothetical next period.

3.4 Fourier Transform

Mostly all the things can be elaborated with the help of a waveform. To view these waveforms, we have the Fourier Transform which is a different and effective approach. It is known that all the waveforms are sums of sinusoids of various frequencies. Here the Fourier Transform plays a vital role as it decomposes a waveform.

This can be further elaborated with the help of an example provided below. Waveforms in the figure are broken down into their constituent frequencies as shown in the rest of the diagrams.

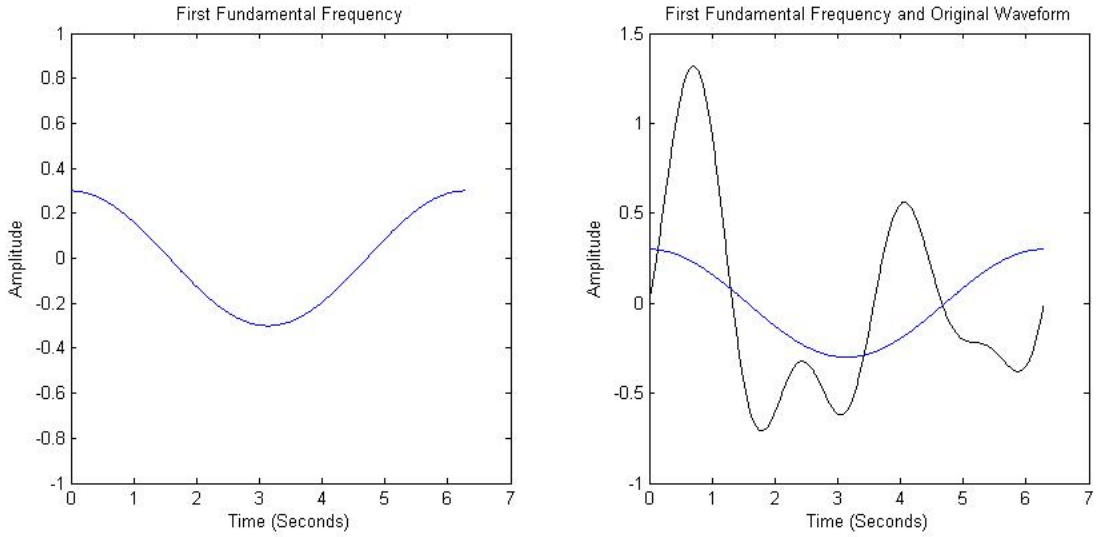

Figure 2:1st fundamental frequency and original waveform

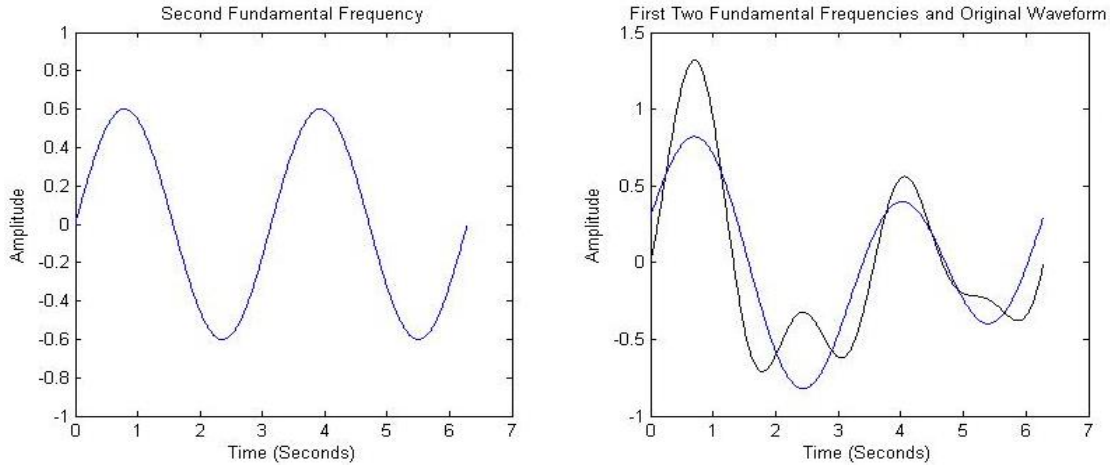

Figure 3: 2nd fundamental frequency and original waveform

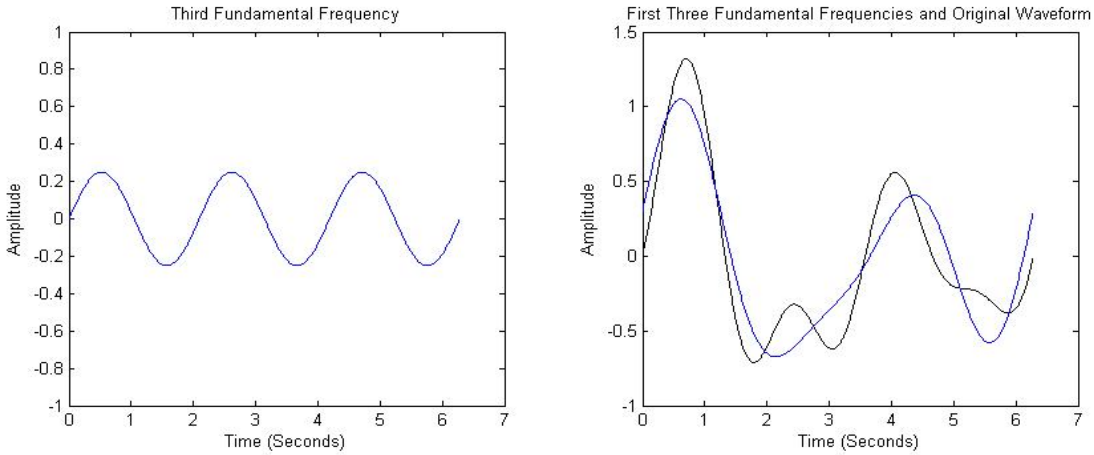

Figure 4: 3rd fundamental frequency and original waveform

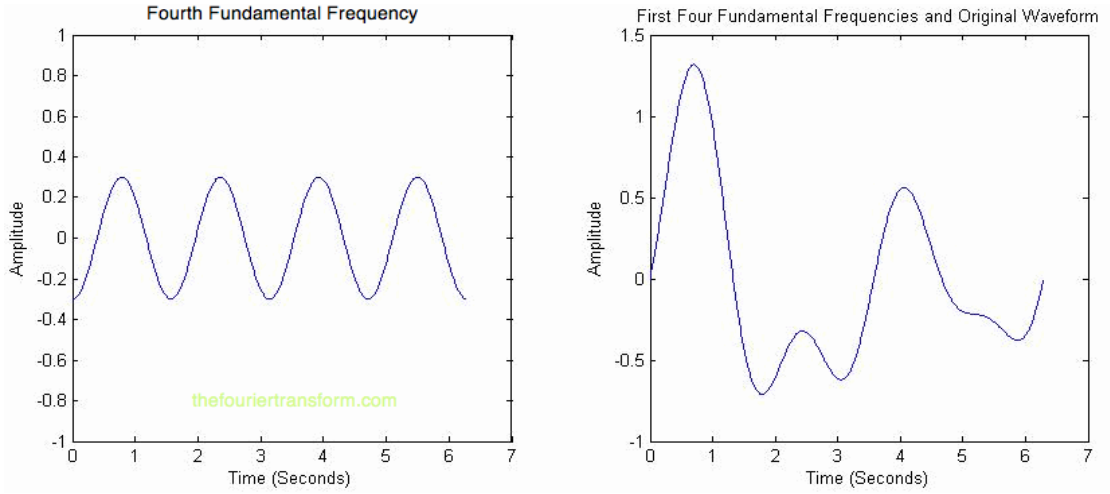

Figure 5: 4th fundamental frequency and original waveform

Fourier Transform has great scope and applications in various fields.

3.5 Discrete Fourier Transform

Discrete Fourier Transform (DFT) can be expressed as:

$$x[k] = \sum_{n=0}^{N-1} x[n] e^{\frac{-j2\pi kn}{N}}$$

To find the DFT of a discrete signal X(***n***) we multiply each value by e raised to some function of ***n***. Where ***n*** is the size of its domain. Then all the results are summed for the given ***n***.

DFT Example:

Let continuous signal be

$$f(t) = \underbrace{5}_{\text{dc}} + \underbrace{2\cos(2\pi t - 90^o)}_{1\text{Hz}} + \underbrace{3\cos 4\pi t}_{2\text{Hz}}$$

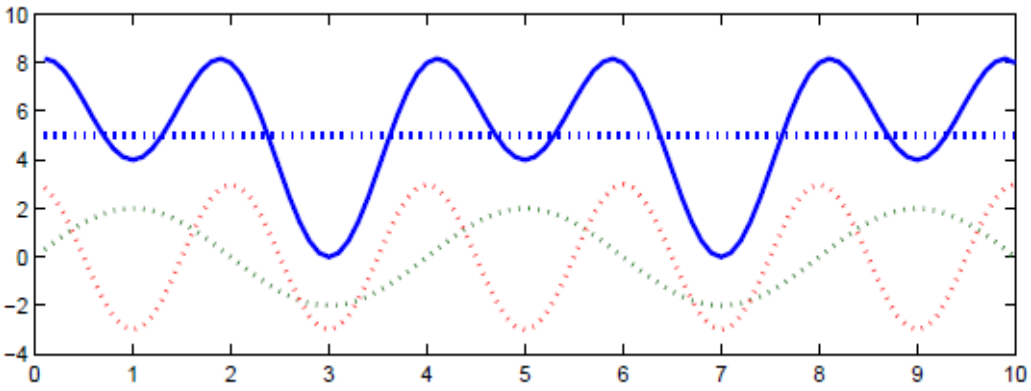

Figure 6:Example Signal for DFT

Let us sample f(t) at 4 times per second (i.e. f=4Hz) from t=0 to t=3/4.

The values of the discrete samples are given by:

$$f[k] = 5 + 2cos(\tfrac{\pi}{2}k - 90^o) + 3cos\pi k \qquad \text{by putting } t = kT_s = \tfrac{k}{4}$$

i.e. $f[0] = 8, f[1] = 4, f[2] = 8, f[3] = 0, \qquad (N = 4)$

$$\text{Therefore} \quad F[n] = \sum_{0}^{3} f[k]e^{-j\frac{\pi}{2}nk} = \sum_{k=0}^{3} f[k](-j)^{nk}$$

$$\begin{pmatrix} F[0] \\ F[1] \\ F[2] \\ F[3] \end{pmatrix} = \begin{pmatrix} 1 & 1 & 1 & 1 \\ 1 & -j & -1 & j \\ 1 & -1 & 1 & -1 \\ 1 & j & -1 & -j \end{pmatrix} \begin{pmatrix} f[0] \\ f[1] \\ f[2] \\ f[3] \end{pmatrix} = \begin{pmatrix} 20 \\ -j4 \\ 12 \\ j4 \end{pmatrix}$$

The magnitudes of DFT coefficients are below:

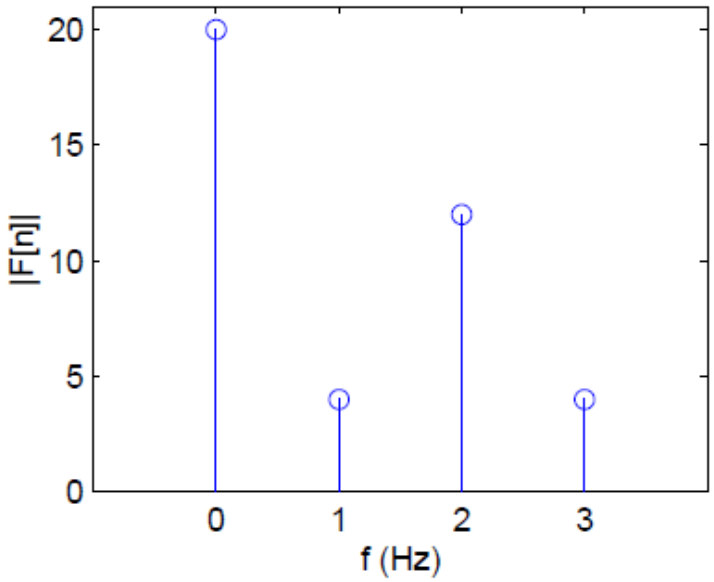

Figure 7: DFT Magnitudes

DFT is only an approximation since it provides only for a finite set of frequencies. There are two main errors of DFT:

1) Aliasing
2) Leakage

3.6 Fast Fourier Transform

Fast Fourier Transform (FFT) is an algorithm as its name implies. It finds the Discrete Fourier Transform of an input at a much faster rate than its direct computation. The Fast Fourier Transform lowers the number of computations required for a problem of size N from O(N^2) to O(NlogN).

Discrete Fourier transform $O\left(N^2\right)$

Fast Fourier transform $O\left(Nlog_2N\right)$

Consider N=8

$$W_8^1 = e^{-j\frac{2\pi}{8}} = e^{-j45^o} = \frac{1-j}{\sqrt{2}} = a, \text{ say.}$$

Then $a^2 = -j$ $a^3 = -ja = -a^*$ $a^4 = -1$

$a^5 = -a$ $a^6 = j$ $a^7 = ja = a^*$ $a^8 = 1$

It is observed that

$$W_8^4 = -W_8^0$$
$$W_8^5 = -W_8^1$$
$$W_8^6 = -W_8^2$$
$$W_8^7 = -W_8^3$$

3.7 Zero-Padding:

The Fourier transform is a frequency-resolution-infinite transformation of an indefinitely long duration signal. The observed frequency of a discrete-time signal is estimated by converting a signal of finite duration T into a number of distinct readings in the frequency response with an accuracy of 1/T. Zero-padding is a method that

enables the DFT to estimate a good prediction of the FT of a waveform. A series of zeros are introduced to the start and the end of the time series first before DFT is determined.

Determining the DFT of the numbers other than integers values of parameter m can be regarded as the result of inserting these zeros. If the input is zero-padded to duration N, then the DFT formula will become:

$$C_{m^*} = \frac{1}{\alpha T} \sum_{n=-\alpha N/2+1}^{\alpha N/2} x_n \mathrm{e}^{-\mathrm{j}2\pi m^* n/(\alpha N)}$$

Here, parameter m is an integer ranging between N/2+1 to N/2, and the signal's time frame is raised from T to αT. Because the input signal is 0 outside the region of −N/2 + 1 ≤ n < N/2, it can be refined:

$$C_{m^*} = \frac{1}{\alpha T} \sum_{n=-N/2+1}^{N/2} x_n \mathrm{e}^{-\mathrm{j}(2\pi n/N)(m^*/\alpha)}$$

This is similar to the previous equation without zero-padding (although expanded by 1/α), however now m accepts numbers in increments of 1/α rather than increments of this one from N/2 + 1/ to N/2. As a result, rather than 1/T, the frequency increments are 1/(αT).

Figure 1 illustrates the DFT (adjusted to use the WFT's highest value) of a complex-valued waveform with frequencies 5/T and the time T, recorded at a rate of 20/T. In the time-frequency domain, we have twenty points, and on the other hand, in the frequency domain also, twenty points are here. In the time-frequency domain, we have twenty points, and on the other hand, in the frequency domain also, twenty points are here.

The estimated frequency band is 9/T to 10/T, with a 1/T resolution among nodes (as this signal has lasted for time T). Figure 1 is also showing the effect of zero-padding, in this zero-padding, changes the length of the signal to double from its previous length. This results in 1/2T frequency resolution and also gives a frequency range of 9.5/T to 10/T. This figure also shows the zero-padding as well as the effect of zero-

padding to four times its original length, resulting in 0.25/T frequency resolution and a frequency range of 9.75/T to 10/T. The very same approximation is obtained with infinite zero-padding as with a windowed continuous FT.

In this case, zero-padding the signal is represented to lead to a decrease of precision in the signal's frequency components. No observed frequency except at 5/T was expected without zero padding. This instance, meanwhile, is a special instance in which the signal's frequency is approximately the same as the other frequency ranges. As a result, while increasing the zero-padding emphasises the fundamental sinc function created by windowing the temporal signal to a finite length, it has no effect on the projected frequencies.

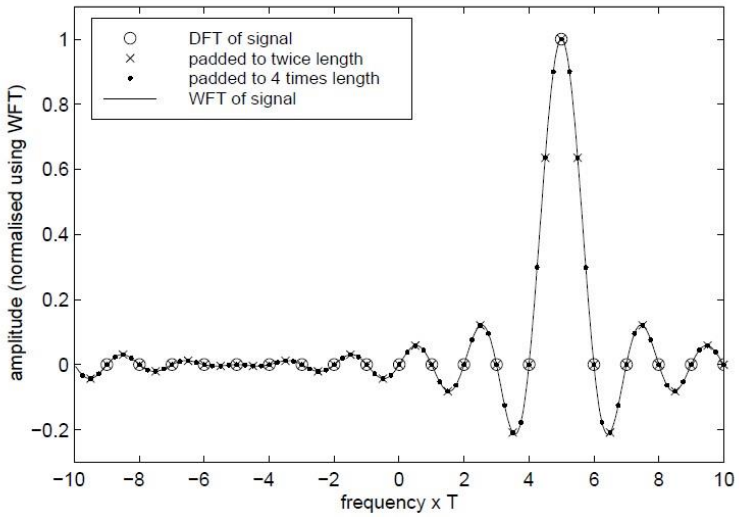

Figure 8:Zero-padded DFT of 5/T frequency complex exponential signal

If indeed the frequency is just not equal to one of the open back signal's frequency ranges, zero-padding will enhance frequency prediction. The Fourier transformation for the 5.2/T complex-valued signal continuing for time T is shown in Figure 3.5. The anticipated frequency without zero padding is 5/T. Nevertheless, as the fundamental sinc function is shown in greater detail with greater resolution, the frequency estimation improves.

This should be emphasized that zero-padding is only able to display a better result in a lower to the constant FT of a windowed signal, and hence is not a true gain in frequency approximation. Only by expanding the duration of the time series and therefore decreasing the size of the sinc function's peaks can actual resolution be

improved. Fig.1 shows the frequency contents projected for the 5/T frequency signal versus frequency estimate whenever the signal is zero-padded to double its initial length and captured over double its initial length. The smooth and dashed lines indicate an endlessly padding signal of length T and 2T, correspondingly, showing all of the subtleties of the fundamental sinc function generated by the temporal windowing.

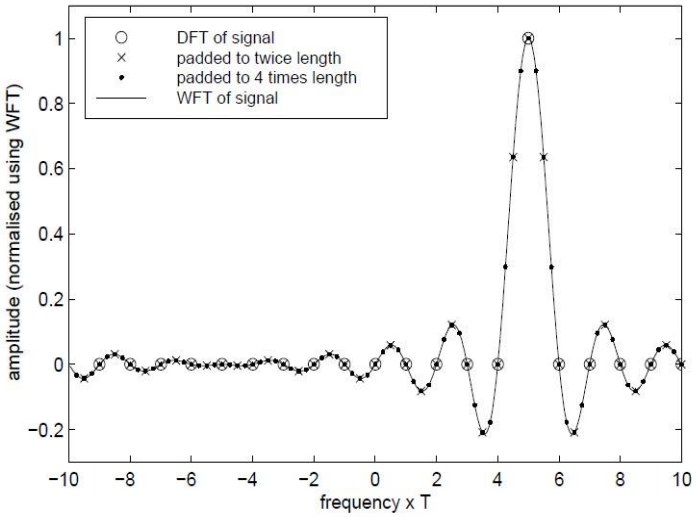

Figure 9: Zero-padded DFT of 5.2/T frequency complex exponential signal

Apparently, the frequencies of the signal may be discovered properly by zero-padding to a sufficient size and searching for the frequency bins with the biggest frequency response. If there are 2 or even more modes, though, the sinc functions belonging to each mode might conflict, resulting in inaccurate predictions of the modes' frequency. Whether a signal of T length in the range from 0 to T is evaluated, it is required to verify that the repetitive signal (that uses the Fourier series technique) includes the real signal across the range from 0 to T in order to retain the right aspect connection. The signals can then be used to determine the DFT throughout the range T/2 to T/2. For instance, if the signal is to be zero-padded to quadruple times its initial length, the repeated signal will have the value 0 over the region 2T to 0, and the input signal will take the price value 0 over the range of 0 to T, and the input signal will take the value 0 over the range T to 2T.

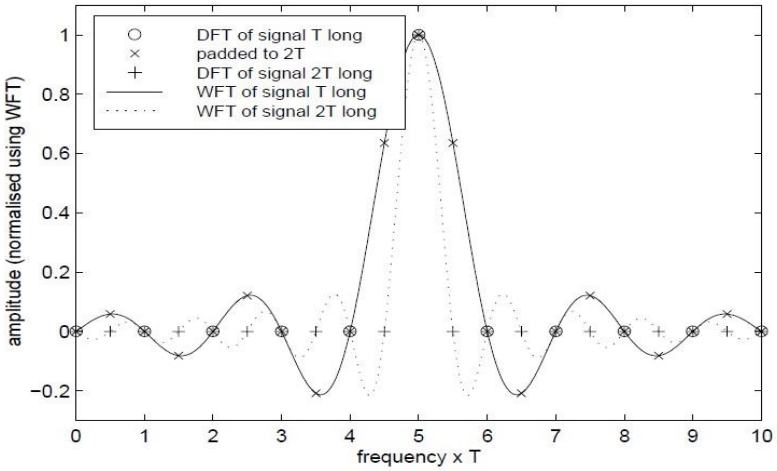

Figure 10: A comparison between zero-padding and an increase in sample time

3.8 Decimation:

To accelerate up data processing, it's often advantageous to lower the sampling rate of signals. The information loss relevant to high-frequency content is the expense of this procedure. To eliminate ambiguity, signals must be filtered while omitting sets of data to eliminate the high frequencies portions, a procedure known as decimation. A Chebyshev low-pass filter is employed in this decimation process, which is a typical MATLAB method.

3.9 Windowing:

Windowing is frequently used to decrease shoulder. First, before DFT is determined, the signal is amplified by a window with the same duration as the input. When considering the windowed Fourier transform, employing the window has the consequence of replacing the rectangular window imposed on the signal. As a result, rather than being convolved with such a sinc function, the frequency is combined with the window's transformation. There seem to be a variety of windows, including the Hanning and Blackman windows, which are very prominent in MATLAB software. Figures 3.7a and 3.7b show the windows in the time domain and frequency domain, as well as a rectangular window for comparisons. The disadvantage of lowering the shoulder would be that the actual frequency peak becomes broader. The approach

provided here does not employ windowing because an accurate frequency estimate is more critical than side-lobe elimination, as the fundamental frequency predominates the input signal.

CHAPTER 4

Theory of Vibrating Wire Strain Gauge

The basic principle of the experiment is based on the fundamental frequency of stationary waves in the wire that is fixed at both ends. The fundamental frequency of the wire may get changed due to the effect of temperature. The concept of a stationary wave in a stretched string and the effect of temperature on its fundamental frequency is discussed below in detail.

4.1 Stationary Wave:

The resultant wave produced by the superposition of two identical waves traveling in opposite directions is called a stationary or standing wave. Consider the superposition of two waves along a string in opposite directions. The picture of such two waves at instants t=0, t=T/2, t=3T/2, and t=T is shown in the figure below. Where T is the time period of the stationary wave.

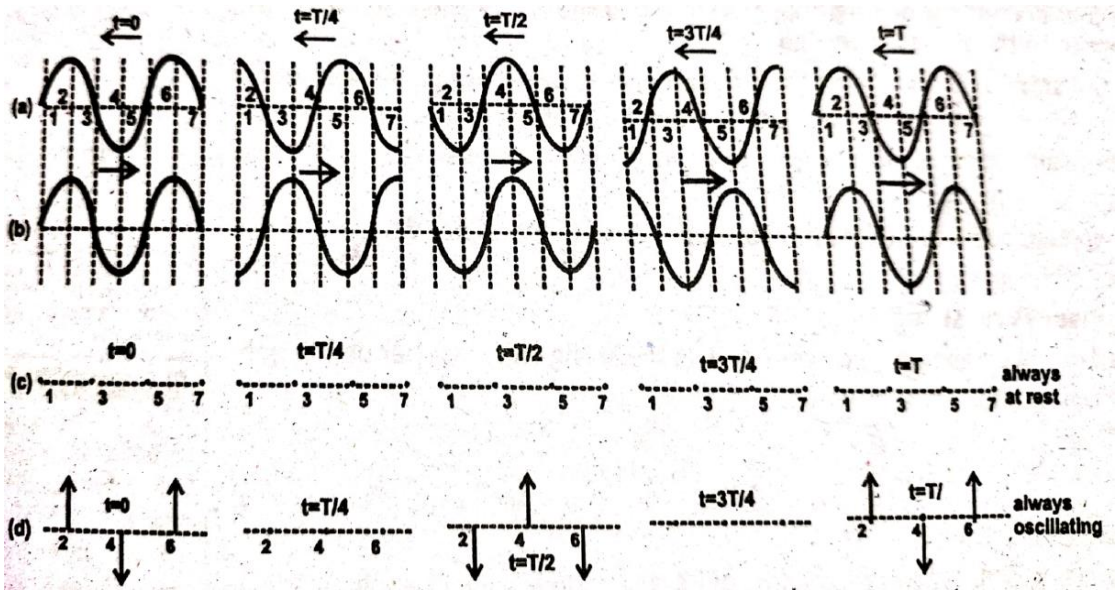

Figure 11: Vibration Nodes

We are interested in finding out the displacement of the points 1,2,3,4,5,6, and 7 at these instants as the waves are superposing at these points. From the above figure, it is obvious that the points 1,2,3,4,5,6, and 7 are distant λ/4 apart, λ being the wavelength of the stationary wave. The resultant displacement at these points can be calculated by applying the superposition principle.

It can be seen that the resultant displacement of the points 1,3,5, and 7 at instants t=0, t=T/2, t=3T/2, and t=T is zero. These points of the medium or string are known as nodes. We can see from the figure (c) that λ/2 is the distance between two connective nodes. The points between the two successive nodes are in phase with each other.

The resultant displacement of the points 2,4, and 6 at instants t=0, t=T/2, t=3T/2, and t=T is the sum of the amplitudes of the component waves. These points of the medium or string are known as antinodes. We can see from the figure (d) that λ/2 is the distance between two connective nodes. The distance between successive and antinode is λ/4.

The energy in a wave moves due to the motion of particles in the medium. The nodes are the points that remain at rest so there is no energy flow through these points. Hence energy remains standing in the medium between two consecutive nodes. Although energy can change its form from kinetic to potential and from potential to kinetic in this portion of the medium. Talking about the antinodes when they are at their extreme positions the energy stored is wholly potential and when they are at equilibrium or mean positions the energy is wholly kinetic.

4.2 Stationary Waves in a String Fixed at Both Ends:

Suppose we have a string of length l. It is stretched and is clamped at its two ends. The tension in the string is denoted by F.

When the string is plucked and then released, two waves are generated which move in opposite directions along the string. Both of these waves are reflected from the clamped ends of the string with the opposite phase to generate stationary waves on the string. As both ends are clamped with rigid supports, these do not vibrate, and we get nodes at the ends.

The speed of the wave depends upon the tension F in the string and mass per unit length or linear mass density of string which is denoted by m.

$$v = \sqrt{\frac{F}{m}} \text{ ---------- (1)}$$

4.2.1 The first mode of vibration

When the string is plucked at the middle of its length then the string vibrates in a single loop as shown in the figure. Such a mode is called the first or fundamental mode of vibration

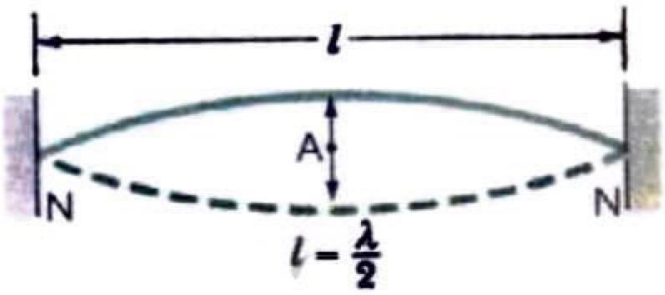

Figure 12: First Mode of Vibrations

Distance between two successive nodes = λ/2

If λ1 be the wavelength and f1 be the frequency of the vibration in this mode, then

$$l = 2\lambda_1$$

$$\lambda_1 = 2l \text{---------- (2)}$$

The speed of the wave will be

$$v = f_1\lambda_1$$

$$f_1 = \frac{v}{\lambda_1}$$

putting values of λ1 we get

$$f_1 = \frac{v}{2l} \text{ ---------- (3)}$$

putting values of v from equation (1) in equation (3) we get

$$f_1 = \frac{1}{2l}\sqrt{\frac{F}{m}}$$

4.2.2 The Second mode of vibration

When the string is plucked from one-quarter of its length then the string vibrates into two loops as shown in the figure below. If λ_2 be the wavelength and f_2 be the frequency of the vibration in this mode, then

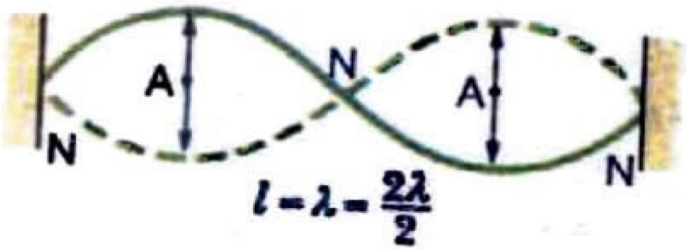

Figure 13: : Second Mode of Vibrations

$$l = \frac{\lambda_2}{2} + \frac{\lambda_2}{2}$$

$$\lambda_2 = l$$

The speed of the wave will be

$$v = f_2\lambda_2$$

$$f_2 = \frac{v}{\lambda_2}$$

Putting values of λ_2 we get

$$f_2 = \frac{v}{l}$$

$$f_2 = \frac{2v}{2l}$$

$$f_2 = 2f_1$$

Hence when the string vibrates in two loops its frequency is twice the frequency when it vibrates in one loop. f_2 is called the first overtone or the second mode of vibration.

4.2.3 The third mode of vibration

When the string is plucked from one-sixth of its length then the string vibrates into three loops as shown in the figure below. If λ_2 be the wavelength and f_3 be the frequency of the vibration in this mode, then

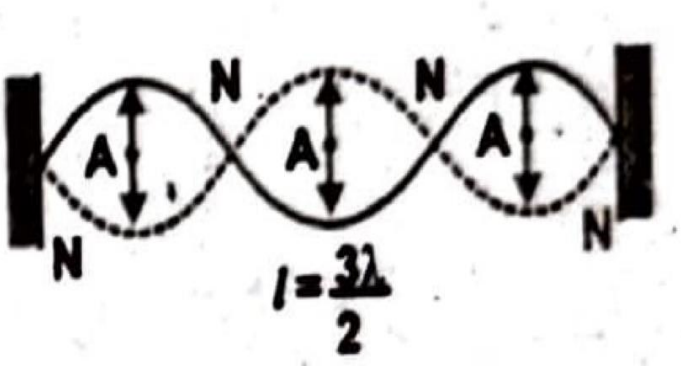

Figure 14: Third Mode of Vibrations

$$l = \frac{\lambda_3}{2} + \frac{\lambda_3}{2} + \frac{\lambda_3}{2}$$

$$\lambda_3 = l$$

The speed of the wave will be

$$v = f_3\lambda_3$$

$$f_3 = \frac{3v}{2\lambda_3}$$

Putting values of λ_2 we get

$$f_3 = \frac{v}{l}$$

$$f_3 = \frac{3v}{2l}$$

$$f_3 = 3f_1$$

Hence when the string vibrates in three loops its frequency is three times the frequency when it vibrates in one loop. f_3 is called the second overtone or third mode of vibration. For the nth mode of vibration frequency of vibration will be

$$f_n = nf_1$$

So, the stationary waves have a discrete set of frequencies which is known as harmonic series. The frequency f1 is known as the fundamental frequency and the other is called overtones.

4.3 Frequency Strain Relationship:

If a wire is held rigidly at both ends the expression for its fundamental frequency can be derived using the principle of stationary waves discussed above

$$v = \sqrt{\frac{Fxl}{m}}$$

$$v = \sqrt{\frac{F}{m/l}}$$

Dividing up and down by Area A

$$v = \sqrt{\frac{F/A}{m/V}}$$

$$v = \sqrt{\frac{\sigma}{\rho}}$$

Here

- A = Area of wire
- V = Volume of wire
- ρ = density of the wire
- σ = Stress the wire

As we know the relationship between frequency and speed for the first mode of vibration is

$$f_1 = \frac{v}{2l}$$

$$f_1 = \frac{1}{2l}\sqrt{\frac{\sigma}{\rho}}$$

For the nth mode of vibration

$$f_n = \frac{n}{2l}\sqrt{\frac{\sigma}{\rho}}$$

4.3.1 Strain in Specimen:

For a specimen shown in the figure below

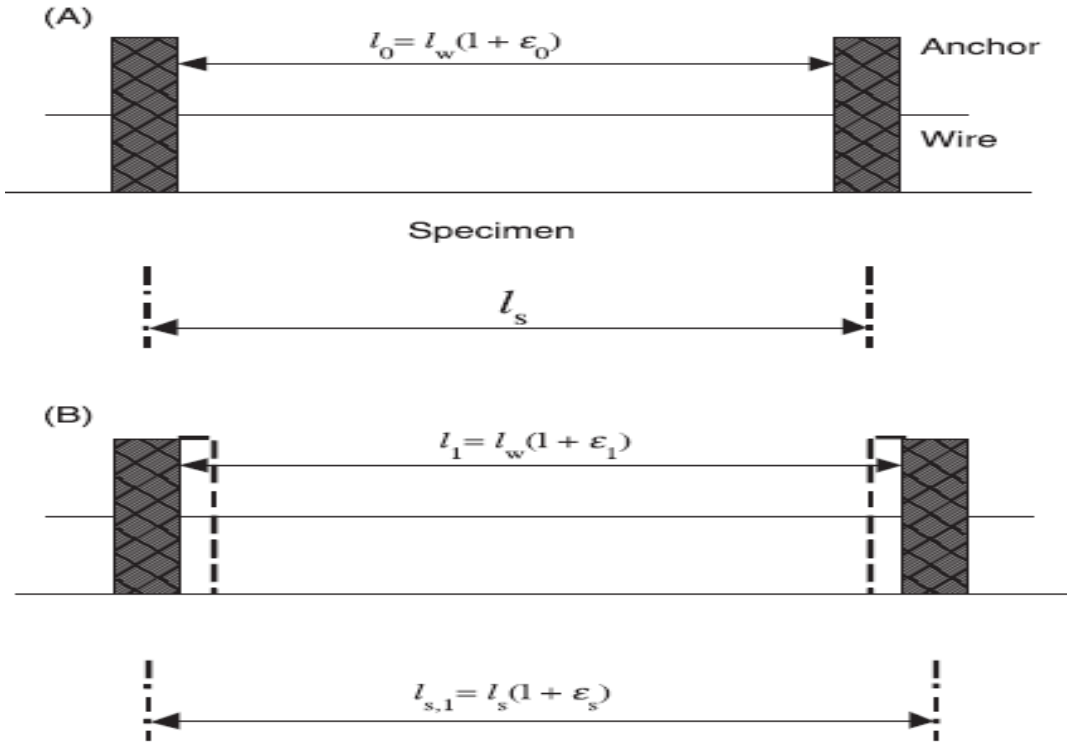

Figure 15: Strained and Unstrained specimen

- Lw =Unstretched length
- l0 = total span held at tension
- E = Modulus of Elasticity

$$f_0 = \frac{1}{2l_0}\sqrt{\frac{E\epsilon_0}{\rho}}$$

Where

$$\epsilon_0 = \frac{l_0 - l_w}{l_w}$$

After loading

$$\varepsilon_1 = \frac{l_1 - l_w}{l_w}$$

And its natural frequency will be

$$f_1 = \frac{1}{2l_1}\sqrt{\frac{E\varepsilon_1}{\rho}}$$

Strain in the specimen is

$$\varepsilon_s = \frac{l_{s,1} - l_s}{l_s} = \frac{l_1 - l_0}{l_s}.$$

The ratio of frequencies before loading and after loading is

$$\frac{f}{f_0} = \frac{l_0}{l}\sqrt{\frac{\epsilon}{\epsilon_0}}$$

Using above expressions

$$\frac{f}{f_0} = \frac{1}{1 + \frac{l_s}{l_0}\epsilon_s}\sqrt{1 + \frac{l_s}{l_w}\frac{\epsilon_s}{\epsilon_0}} \simeq \sqrt{1 + \frac{l_s}{l_w}\frac{\epsilon_s}{\epsilon_0}}$$

Considering $\frac{1}{1 + \frac{l_s}{l_0}\epsilon_s}$ is equal to unity as strain in the wire and specimen is way less than zero so

$$\frac{f_1}{f_0} = \frac{l_0}{l_0 + l_s\varepsilon_s}\sqrt{1 + \frac{l_s\varepsilon_s}{l_w\varepsilon_0}}.$$

Rearranging

$$\epsilon_s = \frac{l_0\epsilon_0}{l_s f_0^2}(f^2 - f_0^2) = G(f^2 - f_0^2)$$

Where G is the gauge factor. Its value only depends on the material of the wire and is independent of the initial strain in the wire or specimen. The value of the gauge factor can be determined theoretically by

$$G = \frac{l_0\epsilon_0}{l_s f_0^2} = \frac{4l_0^3\rho}{l_s E}$$

Normally, the value of the gauge factor is calculated through experimental calibration which will be explained in the coming chapters.

4.4 Effect of Temperature:

Suppose we have temperature variation between the two frequency readings. If the coefficients of thermal expansion of wire and specimen are the same there will be no change in the strain as both specimen and wire will expand with the same factor. On the other, if coefficients of thermal expansion of wire and specimen are different then

the effect of temperature on strain becomes significant. An additional strain will generate due to temperature. It is mandatory to have two gauges, one is for the loading test and the other is for the measurement of relative change in strain due to temperature. Both gauges should be in an identical operating environment. We will discuss the use of a control gauge in the temperature part. So total strain due to load and temperature can be measured by

$$\epsilon_s = \epsilon_{load} + (T - T_0)(\alpha_m - \alpha_w) = G(f^2 - f_0^2)$$

Where

- T0 = Initial Temperature
- T1 = Final Temperature
- α_s = Expansion coefficients of specimen
- α_w = Expansion coefficients of wire

To eradicate this temperature, we use a control gauge which is help close to the specimen or sample. So above equation will become

$$\varepsilon_s^{\text{load}} = G(f_1^2 - f_0^2 - f_{c,1}^2 + f_{c,0}^2).$$

Where

- f_{co} = frequency of control gauge at T0
- f_{c1} = frequency of control gauge at T1
- f_0 = frequency of loading gauge before straining
- f_1 = frequency of loading gauge after straining

CHAPTER 5

Methodology

The basic process of developing the gauge and using it for damage assessment can be broadly divided into 4 categories:

1. Experimental setup of the gauge
2. Signal Processing
3. Calibration of the gauge
4. Damage assessment using the gauge

5.1 Experimental Setup of the Gauge

The assembly of the vibrating wire strain gauge is quite simple. For the gauge, two M8 bolts were glued onto the concrete surface with the help of epoxy. The center-to-center distance between the two bolts was kept 100 mm corresponding to the crack spacing occurring at the stirrup locations. A hole was drilled next to the bolt head to allow the wire to pass through. A guitar string having a diameter of 0.1" was passed through the bolts and was pre-tensioned to a force of 14.72 N with the help of a spring balance. The wire was clamped by the use of well lubricated washers and by tightening the nut. This allowed for the wire to be held in place at the initial tension. The figure below shows the setup of the gauge as viewed from the top and the side.

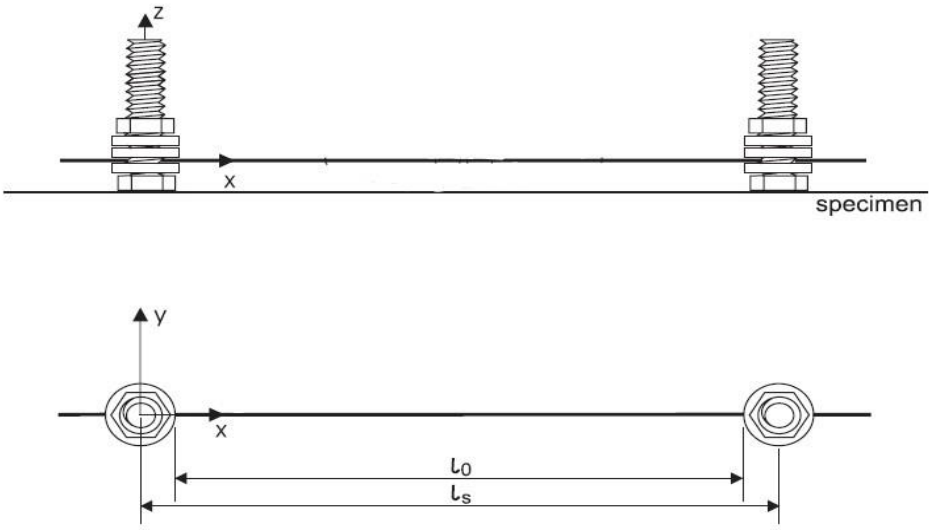

Figure 16: Gauge Setup

As for recording the vibrating wire audio signal, a microphone was clamped onto the bolts near to the string. A low pass filter of 2500 Hz was applied, and the sampling frequency was fixed at 8 KHz. The microphone was then connected to a computer and then the audio was recorded and edited in Ableton (a Digital Audio Workstation). The wire was excited 5 times in succession and then the frequency of each signal was averaged to find out the frequency of the signal. The variation in the frequency content for each strain condition did not deviate by more than ± 0.15%. During this procedure of acquiring the signal, the unstrained control gauge was kept close to the test sample to minimize the effect of temperature on the frequency content of the signal.

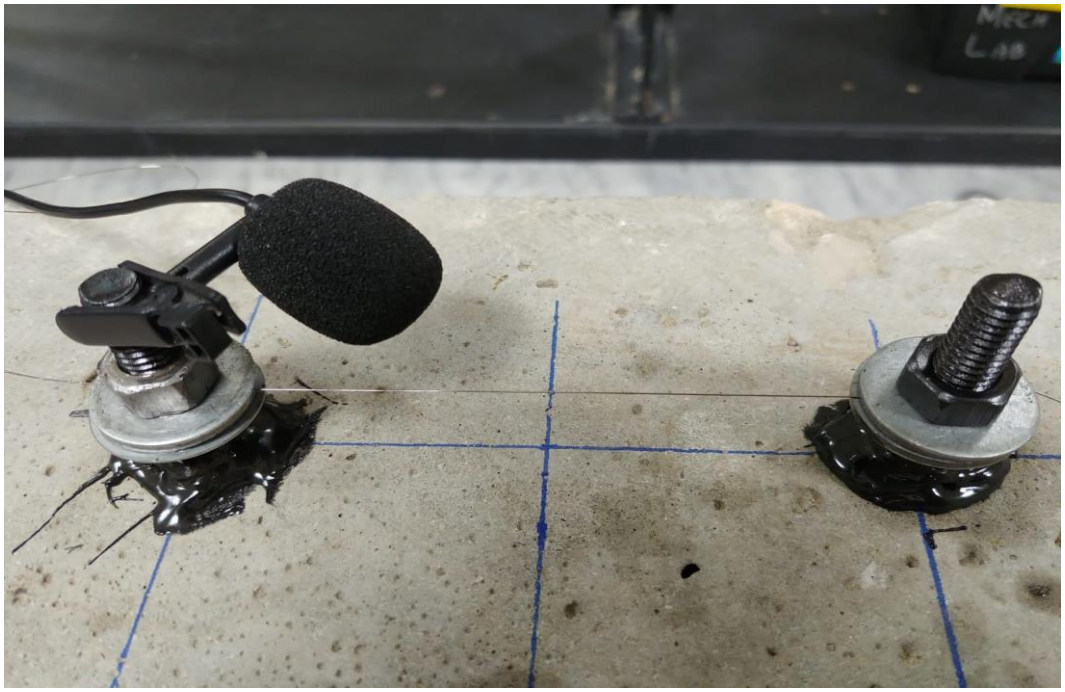

5.2 Signal Processing

The signal was found to be made up of two closely spaced peaks in the frequency domain. A potential reason for this could be because of the difference in stiffness offered by the supports in the y and z directions. The wire was vibrated from the centre in the z-direction but some vibration in the y-direction was inevitable. The figure below shows a typical time-domain signal recorded from the vibrating wire strain gauge. The signal was processed using the software OriginPro.

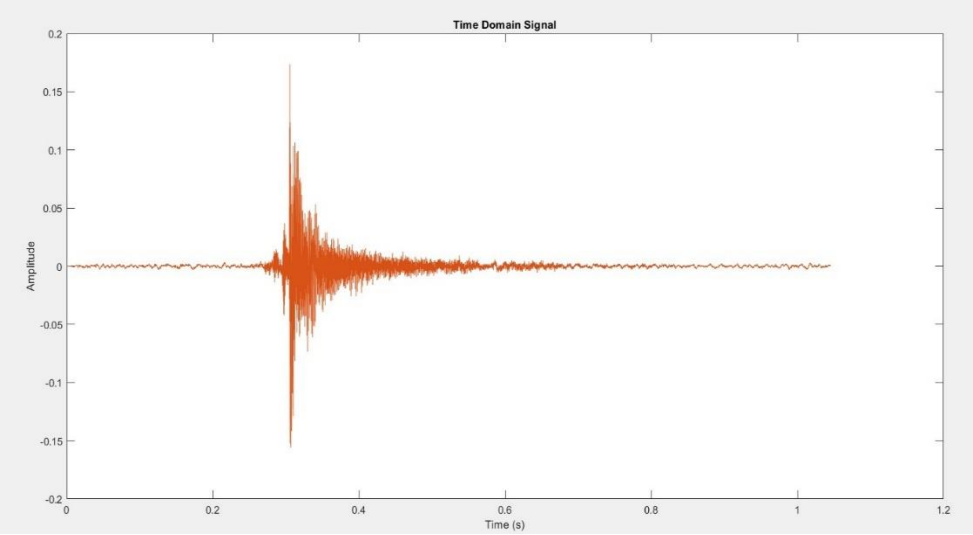

Figure 17: A Typical Time Domain Signal

To determine the frequency content of the signal, the Fast Fourier Transform (FFT) of the signal was performed. The highest frequency peak of the signal corresponded to the frequency of the wire. The figure below shows a typical FFT graph of a signal acquired from the vibrating wire strain gauge. The initial peak has the highest amplitude but is discarded as it corresponds to the background noise. Next, the highest peak in the frequency domain plot is taken as the natural frequency of the wire which in this case turned out to be 902.68 Hz. This frequency for the unstrained gauge could be cross-checked by the theoretical value of frequency for the gauge using the mathematical equation described above. The graph below shows a particular frequency domain plot of the signal.

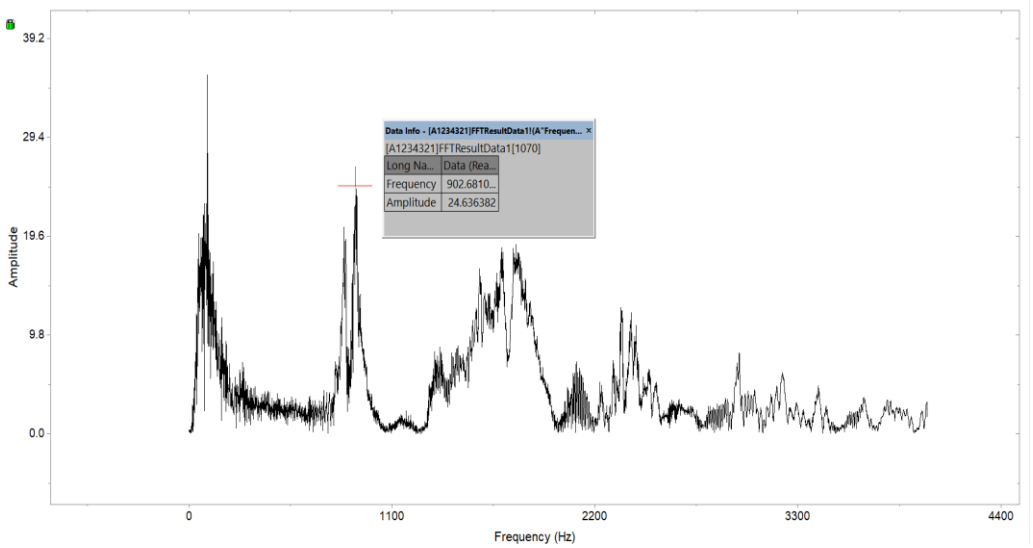

Figure 18:Typical Frequency Domain Plot of Signal

However, since the initial signal is non-linear, it is essential that the non-linear portion of the signal be removed. This was done by determining the time-frequency relationship of the signal. The time-frequency relationship provides information regarding the constituent frequencies that the signal is composed of at a particular time instant. This relationship was determined by the Short-Time Fourier Transform (STFT) of the signal. For the STFT, the Hanning window function having an FFT length of 512 bins and an overlap of 256 bins was selected. Once the time-frequency relationship was obtained, the time till which the signal remains non-linear is removed from the signal and the FFT of the remaining signal is performed for the next 1.5 seconds. After 1.5 seconds the signal-to-noise ratio decreases substantially and so the frequency content cannot be determined accurately (Neild, 2005). The figure below shows an STFT graph obtained from the strain gauge signal.

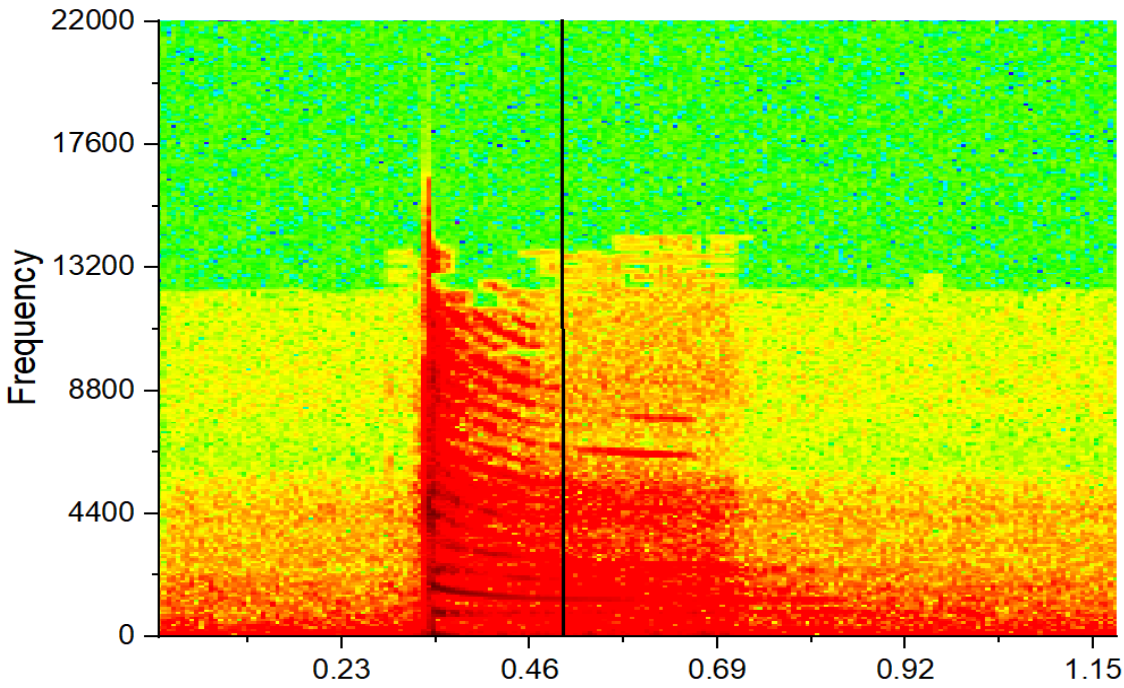

Figure 19:A Typical Frequency-Time Plot of the Signal

It is evident from the graph that the linear signal begins at approximately 0.5 seconds. The amplitude corresponding to the time at which the signal begins to exhibit linear behavior is then identified as the threshold amplitude. The threshold amplitude for each gauge was determined and was kept the same for each loading condition. Once the amplitude of the signal falls below the threshold amplitude, the FFT of the next 1.5 seconds of the signal is done to obtain its frequency content. To filter the signal, a

band pass filter having a bandwidth of 300 Hz was applied centered at the natural frequency of the wire to remove additional noise from the signal. The figure below shows the difference between the time domain plot of the filtered and unfiltered signal.

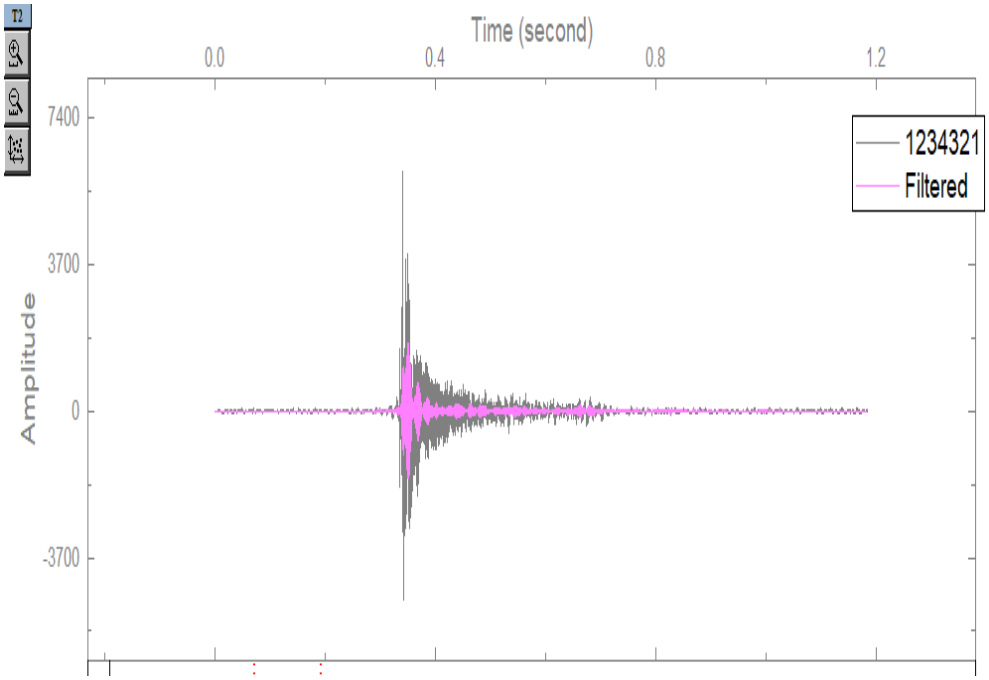

Figure 20:Time Domain Plot of Filtered and Unfiltered Signal

5.3 Calibration of the Gauge

For both the strained and unstrained circumstances, the specimen strain was computed using the reference and measurement gauge frequencies. These frequencies may be combined using equation 6.14 to compute the strain in terms of the gauge factor, G, in comparison to the unstrained state.

Figure 21:Calibration Gauge Setup on Nylon Bar

To calibrate the gauge, tests were conducted on a bar of nylon having cross-sectional dimensions of 16 mm x 16 mm and a length of 300 mm. The Young's Modulus of nylon is 2.7 GPa. Hooks were inserted into the rod at each end and the rod was hanged at one end to allow no moment transfer at the supports. Known loads were applied at the other end by hanging them with the hooks.

Figure 22:Loading Applied on Nylon Bar to Induce Applied Strain

An increment of 5N was applied in each test and the corresponding frequency of the signal was obtained using the same procedure as mentioned above. The change in frequency with incremental load was then determined and a relationship was developed between the factor F (difference in the square of frequencies at strained and unstrained level) and the applied load.

5.4 Damage Assessment using the Gauge

Static strain tests were conducted on the reinforced concrete beams and the strain readings from the vibrating wire strain gauge and demec gauge were compared to cross-validate the accuracy of the strain gauge. The beams were loaded using the 4-point bend test to investigate the effect of pure flexure on the beam. 3 identical reinforced concrete beams having a cross-section of 4” x 6” x 60” were casted using the same mix design. The main reinforcement was #3 bars having a yield strength of 60 psi. The stirrups were #2 bars of 60 psi yield strength being placed at a center-to-center distance of 4”.

Figure 23: Beam Placed on Loading Rig to Induce Damage

Vibrating wire strain gauges were attached at midspan to the beam surface at depths of 1” and 5” from the top of the beam. Demec pips were glued onto the concrete surface on the opposite face of the beam at the same depths corresponding to the location of the vibrating wire gauges. This ensured that both the demec gauge and the vibrating wire strain gauge measured the same strain along the cross-section thereby

allowing validation of the strain measurements made from the vibrating wire strain gauge.

Figure 24: Strain Measurements Using Demec Gauge

The beam was loaded incrementally in a loading rig and the extent and location of cracks were studied. The load was applied in increments of 500 kg till the failure of the beam. Simultaneous readings of strain were taken from both the demec and vibrating wire strain gauges at each damage level.

Figure 25:Cracking Induced in Beam due to Loading

CHAPTER 6

Results and Conclusion

6.1 Gauge Calibration Results

For the calibration of the gauge, different readings were taken at different levels of applied strains. The readings are presented below in the tabulated form.

Gauge Calibration				
Load	**Stress**	**Strain**	**Frequency**	**F**
0	0.0	0.0	955	0.0
10	39062.5	14.5	980.8	49943.6
20	78125.0	28.9	1051.1	192786.2
30	117187.5	43.4	1123.6	350452.0
40	156250.0	57.9	1183.2	487913.6
50	195312.5	72.3	1229.7	600137.1
60	234375	86.8	1290.9	754397.8

From these readings, a graph between the factor F and the applied strain was plotted. The Gauge Factor G is obtained by determining the gradient of the line of best fit between the two variables. The multiplication of the gauge factor with F for any damage level gives us the strain at that damage level.

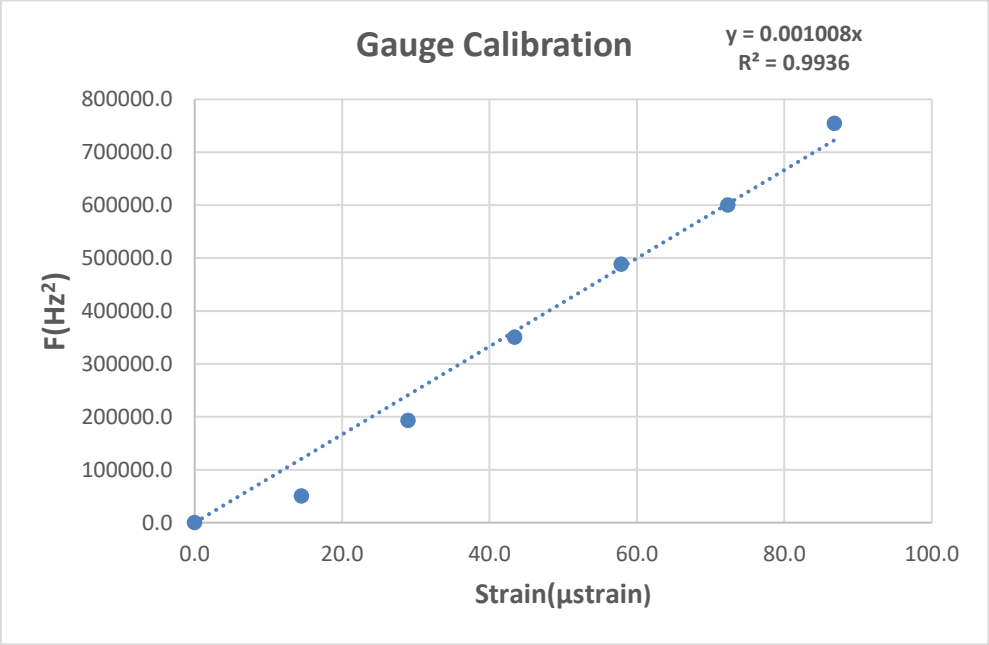

The graph above shows the relationship between F and applied strain. The gauge factor G was determined to be 1.008 x 10^{-9}. The coefficient of determination turned out to be 0.9936. An important point to note here is that the relationship between F and applied strain is linear.

The cross-validation of the strain gauge readings with demec gauge readings was done by 4-point loading on beams. Throughout the testing, the control gauge was placed in the same environment as that of the test beams to minimize temperature differences. The fluctuation in temperatures was not so great so as to affect the readings of both the gauges. The table below shows the values obtained from the demec gauge and the vibrating wire strain gauge.

Beam Test					
Load(kg)	**DG**	**Frequency(Hz)**	**Strain(μstrain)**	**Difference**	**Error (%)**
0	0	902.69	0	0	0
500	640	1197.7	624.6	15.4	2.41
1000	1210	1409.2	1180.4	29.6	2.45
1500	1986	1647	1912.9	73.1	3.68
1794		failure load			

Prior to reaching the 2500 kg damage level, the cracking of the beam caused the gauge to detach from the concrete surface because of which the vibrating wire strain gauge reading was not determined. The average error in the readings was 4.62%. This goes to show that the vibrating wire strain gauge has the ability to accurately measure static strains in structures.

6.2 Conclusion

The use of vibrating wire strain gauge provides a cheap and reliable method for long term damage assessment of structures like bridges, water towers etc. The design and setup of a vibrating wire strain gauge is presented. The vibrating wire strain gauge presented has the capability to measures strain accurately and so can be used for strain measurement purposes in structures.

6.3 Future Recommendations

To further strengthen the design of the gauge proposed, the future work should be aimed at automating the process of signal acquisition and processing which would allow the acquisition of live strain data. This would be particularly useful as it would reduce the tedious task of repeatedly acquiring and processing the signal and would also give strain readings for the present time thereby improving the health monitoring procedure. Another recommendation would be to incorporate a thermistor in the current design of the gauge to remove the need of presence of control gauge near to the test gauge to remove the temperature effects.

References

1. C.R. Farrar and D.A. Jauregui 1998, Smart Materials and Structures, No. 7, 704— 719. Comparative study of damage identification algorithms applied to a bridge; 1, experimental.
2. J.R. Maguire and R.T. Severn 1987, Proceedings of the Institution of Civil Engineering Part 2 83, 769—784. Assessing the dynamic properties of prototype structures by hammer testing.
3. O.S. Salawu 1997, Canadian Journal of Civil Engineering 24, 218—228. Assessment of bridges: use of dynamic testing
4. B.J. Eccles, J.S. Owen, M.A. Woodings and B.S. Choo 1997, Structural Faults and Repair Conference, Edinburgh. A proposed new approach to full life qualitative bridge assessment.
5. M. Abdel Wahab and G. De Roeck 1997, Structural Engineering International 4, 266—270. Effect of temperature on dynamic system parameters of a highway bridge.
6. G.P. Roberts 1995, The Institution of Structural Engineers, Analysis and Testing of Bridges Seminar. Recent experience in dynamic monitoring of a multi-span bridge.
7. H.J. Salane and J.W. Baldwin Jr. 1990, Journal of Structural Engineering 116, No. 7, 2008—2021. Identification of modal properties of bridges.
8. O.S. Salawu and C. Williams 1995, Journal of Structural Engineering 121, No. 2, 161—173. Bridge assessment using forced-vibration testing.
    a. Goldsmith 1999, Fourth Year Undergraduate Project Report, Department of Engineering Science, University of Oxford. Damage detection in concrete beams using vibration measurements
9. K. Van Den Abeele and J. De Visscher 2000, Cement and Concrete Research 30, 1453—1464. Damage assessment in reinforced concrete using spectral and temporal nonlinear vibration techniques.
10. J.S. Owen 2001, Civil Engineering Colloquium, University of Oxford, February 23th. Structural health monitoring of bridges
11. B.J. Eccles, J.S. Owen, B.S. Choo and M.A. Wooding 1999, 4th Conference of the European Association of Structural Dynamics (EURODYN), 357—364. Non-linear vibrations of cracked reinforced concrete beams.

12. D.S. Prakash Rao, M.G. Tamhankar and S.P. Sharma 1983, Materials and Construction 16, No. 96, 457—466. Literature survey on in situ testing of concrete bridges.
13. O.S. Salawu and C. Williams 1995, Engineering Structures 17, No. 2, 113—121. Review of full-scale dynamic testing of bridge structures.
14. M. Raghavendrachar and A.E. Aktan 1992, Journal of Structural Engineering 118, No. 8, 2186—2203. Flexibility by multireference impact testing for bridge diagnostics
15. J.L Humar and A.M. Kashif 1993, Canadian Journal of Civil Engineering 20, 287— 298. Dynamic response of bridges under travelling loads.
    a. Kr¨amer, C.A.M. De Smet and G. De Roeck 1999, Proceedings of the International Modal Analysis Conference (IMAC) 17, 1023—1029. Z24 bridge damage detection tests
16. D.F. Mazurek and J.T. DeWolf 1990, Journal of Structural Engineering 116, No. 9, 2532—2549. Experimental study of bridge monitoring techniques.